Electrostatic and electromagnetic fluctuations detected inside magnetic flux ropes during magnetic reconnection

Wang, Rongsheng; Lu, Quanming; Nakamura, Rumi; Huang, Can; Li, Xing; Wu, Mingyu; Du, Aimin; Gao, Xinliang; Wang, Shui

Published in:
Journal of Geophysical Research: Space Physics

DOI:
10.1002/2016JA022906

Publication date:
2016

Citation for published version (APA):
Wang, R., Lu, Q., Nakamura, R., Huang, C., Li, X., Wu, M., Du, A., Gao, X., & Wang, S. (2016). Electrostatic and electromagnetic fluctuations detected inside magnetic flux ropes during magnetic reconnection. *Journal of Geophysical Research: Space Physics*, *121*(10), 9473-9482. https://doi.org/10.1002/2016JA022906

Electrostatic and electromagnetic fluctuations detected inside magnetic flux ropes during magnetic reconnection

Rongsheng Wang[1*], Quanming Lu[1], Rumi Nakamura[2], Can Huang[1], Xing Li[3], Mingyu Wu[1], Aimin Du[4], Xinliang Gao[1] and Shui Wang[1]

[1]*Key Laboratory of Geospace Environment, Department of Geophysics and Planetary Science, University of Science and Technology of China, Hefei, 230026, China*

[2]*Space Research Institute, Austrian Academy of Sciences, Graz, 8042, Austria*

[3]*Institute of Mathematics and Physics, Aberystwyth University, Aberystwyth, Ceredigion SY23 3BZ, UK*

[4]*Key Laboratory of Earth and Planetary Physics, Institute of Geology and Geophysics, Chinese Academy of Sciences, Beijing, 100029, China*

[*]*rswan@ustc.edu.cn;*

Abstract

A series of magnetic flux ropes embedded in the ion diffusion region of a magnetotail magnetic reconnection event were investigated in this paper. Waves near the lower hybrid frequency were measured within each of the flux ropes, and can be associated with the enhancements of energetic electrons in some of the flux ropes. The waves in the largest flux ropes were further explored in more detail. The electrostatic lower-hybrid-frequency-range

This article has been accepted for publication and undergone full peer review but has not been through the copyediting, typesetting, pagination and proofreading process which may lead to differences between this version and the Version of Record. Please cite this article as doi: 10.1002/2016JA022906

waves are detected at the edge, while electromagnetic lower-hybrid-frequency-range waves are observed at the center of the flux rope. The electromagnetic waves are right-hand polarized and propagated nearly perpendicular to magnetic field lines, with a wavelength of ion-electron hybrid scale. The observations are analogous to simulations in which the electrostatic lower hybrid waves are confined to the edge of current sheet, but can directly penetrate into the current sheet center in the form of the electromagnetic mode. The observations indicate that the electromagnetic lower-hybrid-frequency-range waves can be excited inside magnetic flux ropes.

1. Introduction

Magnetic reconnection is a fundamental physical process in space, astrophysics as well as laboratory plasma, and is believed to be the major reason for a large number of explosive energy release phenomena, such as solar flares, magnetospheric substorms, jets in accretion disks, and sawtooth instability in Tokomaks [*Yamada et al.*, 2010]. In the collisionless plasma environment, anomalous resistivity results from micro-instability turbulence and is supposed to be responsible for mediating magnetic reconnection. The lower-hybrid-drift instability (LHDI) has been invoked as a primary candidate to produce the anomalous resistivity [*Davidson and Gladd*, 1975; *Daughton et al.*, 2004; *Fujimoto et al.*, 2011]. The LHDI is driven by the diamagnetic drift current in the presence of inhomogeneity of the plasma density and magnetic field [*Krall and Liewer*, 1971], and the fastest growing rate peaks at $k\rho_e \approx 1$ for a broad range of frequencices ($\Omega_{ci} < \omega \le \Omega_{lh}$), where Ω_{ci} is proton gyrofrequency, $\Omega_{lh} = \omega_{pi} / (1+\omega_{pe}^2 / \Omega_{ce}^2)^{1/2}$ is the lower-hybrid-frequency, ω_{pe} (ω_{pi}) refers to

electron (proton) plasma frequency, and ρ_e is the electron gyroradius. The linear theory predicts that the fastest growing modes are confined to the edge of the current sheet ($|z| \geq L(T_e/2T_i)^{1/2}$, where z is the distance from the current center in normal direction, L is the thickness of the current sheet, and T_e and T_i are electron and ion temperatures, respectively.) in a modified Harris current sheet [*Davidson et al.*, 1977; *Huba et al.*, 1980]. The lower hybrid waves (LHWs) have been observed by spacecraft measurement [*Bale et al.*, 2002; *Vaivads et al.*, 2004; Zhou et al., 2009 and 2014; *Norgren et al.*, 2012] and in laboratory experiments [*Carter et al.*, 2002 and *Dorfman et al.*, 2013]. Measurements at the magnetopause find that the contribution of the LHDI anomalous resistivity to the parallel electric field is less than 1% of the measured parallel electric field, indicating the LHDI cannot play a significant role in driving reconnection [*Bale et al.*, 2002], Furthermore, even if they are important, their relevance is limited to the separatrices of the reconnection region [*Vaivads et al.*, 2004]. A similar conclusion was also obtained from laboratory experiments [*Carter et al.*, 2002 and *Dorfman et al.*, 2013].

Despite being confined to the edge of the current sheet, the LHDI may play an indirect role in reconnection onset [e.g. *Daughton et al.*, 2004]. A number of numerical simulations [*Winske*, 1981; *Horiuchi and Sato*, 1999; *Daughton*, 2003; *Guo et al.*, 2008] revealed that a significant electromagnetic component can penetrate into the center of the current sheet during the evolution of the LHDI. This longer wavelength electromagnetic LHWs may facilitate onset of magnetic reconnection [*Horiuchi and Sato*, 1999; *Fujimoto*, 2009] and influence its evolution [*Daughton*, 2003; *Roytershteyn et al.*, 2012]. In a stastical study of the waves near the lower hybrid frequency measured in the magnetotail reconnection

region[*Zhou et al.*, 2014], the magnetic field fluctuations are found to increase while electric field fluctuations decrease as the plasma beta (β) increases, and they both disappear when β exceeds 10. Using the observations in the separatrix reigon and at a current sheet center, the electrostatic and electromagnetic fluctuations near the lower hybrid frequency are directly detected, resepctively. However, the observations of the electrostatic and electromagnetic waves are separated by two minutes in a single ion diffusionr egion, and there are multiple crossings of the current sheet between them [*Zhou et al.*, 2009]. Thus, it is hard to say whether they are directly correlated.

In this paper, we revisited the electromagnetic fluctuations reported by *Zhou et al.*, [2009] and find that the electromagnetic fluctuations themselves are bounded by the electrostatic fluctuations. All the electrostatic and electromagnetic fluctuations are confined inside a single large magnetic flux rope. To our knowledge, this type of waves inside a flux rope hasn't been reported before. This type of waves is only detected in the largest flux rope. In other flux ropes observed in the same ion diffusion region, only the electrostatic fluctuations were observed. The role of the waves in controlling reconnection is discussed also.

2. Database

The data from several instruments onboard Cluster [*Escoubet et al.*, 2001] are used in this letter. Magnetic field data sampled at 22/s and electric field data sampled at 25/s are obtained from the FGM [*Balogh et al.*, 2001] and EFW [*Gustafsson et al.*, 2001] instruments, respectively. Magnetic field and electric field spectrogram data from the STAFF instruments [*Cornilleau-Wehrlin et al.*, 2003] are used. Electron energy spectrum data is taken from the

PEACE instruments [*Johnstone et al.*, 1997]. The electron density is derived from the spacecraft potential [*Gustafsson et al.*, 2001]. In this letter, the geocentric solar ecliptic system (GSE) is used to investigate the event associated with the waves.

3. Observation and Analysis

3.1 Overview of the reconnection event

On September 19, 2003, Cluster crossed the current sheet in the near-Earth tail at (-17.5, 3.4, 0.6) R_E and encountered one reconnection event therein [*Borg et al.*, 2005]. Figure 1 shows an overview of the reconnection event. During 23:25-23:34 UT, the proton high speed flow reversed from tailward to Earthward at about 23:30 UT (Figure 1a), accompanied with the reversal of B_z (Figure 1b) from south (negative) to north (positive). In the same interval, B_y displayed a quadrupolar structure in the $v_x - B_z$ plane (Figure 3, in [*Borg et al.*, 2005]). Thus, it is concluded that the spacecraft passed through the ion diffusion region during 23:25-23:34 UT, marked as a horizontal blue bar at the top of Figure 1. The spacecraft detected the reversal point of the high speed flow at about 23:30 UT, with a substantial value of B_x (~10nT) in Figure 1d. Hence, the spacecraft traversed the region north of the X-line. Since Cluster crossed the current sheet several times in the ion diffusion region (Figure 1d), a few papers have studied this event on single or multiple crossings of the ion diffusion region [e.g. *Borg et al*., 2005; *Zhou et al*., 2009; and *Huang et al*., 2012]. *Zhou et al.* [2009] shows the waves near the lower hybrid frequency in crossings of the separatrix region and the current sheet center. *Huang et al* [2012] studied the electron acceleration near a secondary reconnection X-line. Before the high speed ion flows (before 23:24 UT), there was a background guide field in the *y* direction (Figure 1c), its average value was approximate -4

nT. Thus, this guide field directed to dawnward in this reconnection event.

3.2 Magnetic flux ropes inside the ion diffusion region

In this paper, we will mainly focus on a train of magnetic flux ropes detected immediately Earthward of the reconnection X-line between 2331:00 and 2332:40 UT, corresponding to the pink bar in Figure 1b. The flux ropes are also shown in more detail in Figure 2. There exists five magnetic flux ropes encountered by Cluster one after another. The vertical dashed lines correspond to the centers of each of the flux ropes. Essentially, a magnetic flux rope is denoted by the helical magnetic field structure. So, the criteria for identifying magnetic flux ropes in the magnetotail are 1) a bipolar B_z signature (Figure 2c) and 2) an enhanced core field over the background field in the dawn-dusk direction (B_y, Figure 2d). Then, five flux ropes are identified and all of them are embedded within the Earthward burst bulk flows ~ 500 km/s (Figure 1a). For the first (~2131:18 UT), second (2131:25 UT) and fourth (2131:48 UT) flux ropes, their core field was negative and as strong as the amplitude of B_z. In contrast, at the third flux rope (2131:40 UT), the core field (15 nT) was positive and stronger than the amplitude of B_z. As for the last one at 2332:15 UT which was also the largest one (the longest duration, ~ 18s), $|B_y|$ was enhanced up to 10 nT but without a clear peak at its center as the other flux ropes. The reason could be the large disturbance of magnetic field at its center. The disturbance will be further studied later. After the last flux rope, B_x decreased down to -18 nT (Figure 2e).

The spacecraft separation was smaller than 250 km during this interval, so that the Curlometer technique [*Dunlop et al.*, 2002] can be used to calculate the current density on the ion scale (ion inertial length c/ω_{pi} ~ 500 km for $N_e = 0.2\,cm^{-3}$). The current density

($j_{//}$,| $j_{\perp}$ | , Figure 2b) were both enhanced inside the first two flux ropes. Within the third and fourth flux ropes, only the parallel current density was dramatically enhanced and the perpendicular components kept nearly constant. For the last one, the perpendicular current density peaked near its center and the parallel current fell to 0 around its center. The plasma number density (Figure 2a) was enhanced within the first, second, and fifth flux ropes. In the third flux rope, the plasma number density was enhanced also but had a local depression near the flux rope center. For the fourth flux rope, the density was always very low. During the interval shown in Figure 2, all enhancements of the current density were closely associated with one of the flux ropes except the one at about 2331:35 UT when the parallel current density changed sign from negative to positive in association with an enhanced perpendicular current. This thin current layer corresponds to a secondary reconnection X-line rather than a flux rope, as indicated by *Huang et al.* [2012]. So, the flux ropes can be regarded basically as thin filamentary currents.

3.3 Waves within magnetic flux ropes

The Morlet wavelet spectrograms of electric field and magnetic field from 0.1 Hz to 11 Hz are presented in Figures 2g and 2h, respectively. The upper and lower white curves in both panels correspond to the proton gyrofrequency, f_{ci}, and lower hybrid frequency, f_{lh}, respectively. It appears that the electric field fluctuations between f_{ci} and f_{lh} are enhanced within each flux rope. The electric fluctuations are stronger in the first, fourth and fifth flux ropes than the other two ropes (the second and third flux ropes). The magnetic field fluctuations between f_{ci} and f_{lh} show clear enhancement also, but without close correlation to the flux ropes. Analyzing power spectra of the fluctuations within each flux

rope, we find that the waves are primarily electrostatic and the frequencies extend over a broad range from 1.0 Hz to 11 Hz (Figure 2g). Therefore, the electrostatic waves are lower-hybrid-frequency-range waves (LHRWs). In some flux ropes (e.g. the first, second, and fifth flux ropes), the strong cross-field drift currents ($|j_{\perp}|$ Figure 2b) and the significant density gradient (Figure 2a) could be the source of free energy for the observed LHRWs. In other two flux ropes (the third and fourth flux ropes), the parallel current density was very strong and the perpendicular current density was negligible. Thus, the source of free energy for the observed LHRWs in these flux ropes should be different. Inside some of the flux ropes (e.g. the first, second, fourth and fifth), an evident increase of the electron differential fluxes are found between 4 and 10 keV (Figure 2i).

In addition to the electrostatic waves detected inside the flux ropes, more complex fluctuations were detected in the last flux rope. The waveform and wavelet spectrogram data associated with this flux rope are enlarged in Figure 3. The spacecraft traversed this flux rope in the southern hemisphere ($B_x < 0$, Figure 3b). At the beginning of this short period (before 2332:04 UT), the spacecraft was in the edge of the flux rope. From 2332:04 to 2332:13 UT, corresponding to the left pink bar below panel b, B_x progressively increased from -12 nT to -6 nT and B_z gradually rose from negative to zero. Meanwhile, the plasma beta β evolved from 0.5 to 5 (Figure 3a). Therefore, the spacecraft was gradually approaching the center of the flux rope from its edge. During 2332:13-2332:19 UT (the blue bar below the panel b), B_z was close to 0; β reached its maximum value but fluctuated around 6. Thus, the spacecraft was then near the center of the flux rope. After 2332:19 UT, B_x decreased to -10 nT, B_z enhanced to 10 nT, and β reduced to 0.5 with a spike at about 2332:21 UT. Thus,

the spacecraft got into the trailing part of the flux rope. Based on the analysis above, the spacecraft passed through the filament current of the flux rope with a relatively long stay of 7 seconds near its center. The electric field fluctuations were as strong as 100 mV/m in this flux rope (Figure 3c). A large amplitude magnetic field perturbation was detected in the center of this flux rope (the blue bar). According to the wavelet spectrogram, the electric field fluctuations were measured in the entire flux rope (Figure 3d) whereas the magnetic field fluctuations were mainly detected near its center (Figure 3e). The power spectra of the electric field and magnetic field versus frequency for the interval in Figure 3 are displayed in Figure 4. The clear peaks for both electric field and magnetic field were observed at ~ 2 Hz, lower than the lower hybrid frequency f_{lh}, and corresponded to the electromagnetic waves in the flux rope center. Enhancements near the lower hybrid frequency (3~50 Hz) were only measured in the electric field, which corresponds to the electrostatic waves detected in the boundary regions of the flux rope (the pink bar below Figure 3b). Since only two components of electric field were measured by Cluster, properties of the electrostatic waves cannot be resolved in further detail.

The details on the electromagnetic waves in the filament current center are shown in Figure 5. Figure 5a displays the density at C2. Figures 5b and 5d show magnetic field variations ($\delta\mathbf{B}$) in the GSE coordinates and in the field-aligned coordinates, respectively. It can be found that the magnetic field fluctuated in all three components ($\delta B_x \sim \delta B_y > \delta B_z$, Figure 5b) but primarily in the parallel direction (Figure 5d). Since the electromagnetic waves were detected by all four satellites and are almost monochromatic, the Timing method [e.g. Schwartz 1998] can be used to calculate its propagating direction and velocity. The Timing analysis was

performed to δB_y during 2332:15 ~ 2332:19 UT. The propagation direction ($\mathbf{k}$) and velocity ($\mathbf{v}$) of the waves was estimated to be (0.807, -0.591, 0.014) and (520.8, -381.1, 9.06) km/s in the spacecraft frame. The wave propagation angle with respect to ambient magnetic field was about 95^o. Thus, the waves were propagating nearly perpendicular to magnetic field and the wave length was about 391 km. During 2332:15 ~ 2332:19 UT, the geometrical shape of the Cluster spacecraft is close to regular tetrahedron and the wave speed is much faster than the Cluster speed, therefore the errors of the Timing analysis mainly arises from the uncertainties of the time lag between various satellites [e.g. *Zhou et al*., 2009]. Using the equation (1.7) in the ref. [*Sonnerup et al*., 2008], the maximum uncertainty of the time lag is only about 0.01s (between C1 and C3), which is much short than the time lag of about 0.30 s. Thus, the Timing results are reliable. The density perturbation (Figure 5a) was related with the electromagnetic fluctuations and therefore the fluctuations should be the compressional waves.

The Cluster spacecraft only measures the electric field components E_x and E_y (Figure 5c) in the spacecraft spin plane. Thus, the parallel electric field and the perpendicular electric field can only be estimated, if the magnetic field was lying in this plane. In order to confirm whether the parallel electric field can be estimated here, we calculated the angle between the ambient magnetic field and the spacecraft spin plane and showed it in Figure 5e. It can be seen that the angle was smaller than 5^o between 2332:12 and 2332:15 UT. In other words, the parallel and perpendicular electric field estimations may be considered substantially reliable during this short span. Quantities $E_{//} = \mathbf{E}\cdot\mathbf{B}/|\mathbf{B}|$ and $(E_\perp)_y$ ($E_\perp = \mathbf{B}\times(\mathbf{E}\times\mathbf{B})/|\mathbf{B}|^2$) are presented in Figure 5f. The parallel electric field fluctuations were intermittently observed in

the electrostatic wave (2332:11-2332:13 UT) and also in a short period of the electromagnetic waves (after 2332:13 UT), but were much weaker than the perpendicular component.

Figure 6 shows the polarization of the electromagnetic waves using the data in the interval 2332:13.8-2332:14.5 UT when the waves began to be detected. The two components are obtained from the equations: $\hat{\mathbf{k}}_{\perp 1} = \hat{\mathbf{k}} \times \hat{\mathbf{B}}$ and $\hat{\mathbf{k}}_{\perp 2} = \hat{\mathbf{k}} \times \hat{\mathbf{k}}_{\perp 1}$, where the $\wedge$ script denotes the unit vector. It is clear that the waves are elliptically right-hand polarized. In our event, the wavelength of the electromagnetic wave was estimated to be 391 km $\approx 4.5\sqrt{\rho_i \rho_e}$, where $\rho_i \approx 847km$ and $\rho_e \approx 9km$. The relative drift velocity was $v_{drfit} = j_\perp / eN \approx$ 938 km/s, where $j_\perp \approx$ 30nA/m^2. The ratio between the wave phase velocity ($v_{phase} \sim$ 645km/s) and the drift velocity is about 0.68. Considering the Doppler Effect, the wave frequency in the plasma frame was modified slightly and the effect does not change our conclusion.

4. Discussion and Summary

Numerical simulations of the LHDI instability predict that electromagnetic waves can be excited in the current sheet center [e.g. *Daughton*, 2003]. Using the linear Vlasov theory and particle-in-cell simulations, Daughton [2004] concluded that the electromagnetic wave is one significant component of the LHDI with a longer wavelength ($k\sqrt{\rho_i \rho_e} \sim 1$) than the electrostatic lower hybrid waves ($k\rho_e \sim 1$) confined in the edge of the current sheet. In our event, the electromagnetic waves are surrounded by the electrostatic waves and are observed in the center of one flux rope. The electromagnetic waves were propagating obliquely to magnetic field with a phase speed comparable to the drift velocity ($\frac{v_{phase}}{v_{drift}} \sim 0.68$), and the wavelength of the electromagnetic wave was estimated to be the ion and electron hybrid scale

($4.5\sqrt{\rho_i\rho_e}$). All of these features of the electromagnetic fluctuations are *in* accordance to the simulation results and also the experimental results from MRX [*Ji et al.*, 2004]. In these experiments [*Ji et al.*, 2004], the magnitude of the electromagnetic fluctuations and enhancement of reconnection rates display a positive correlation and the electromagnetic waves were identified as a right-hand polarized whistler wave branch. Moreover, the electromagnetic waves in the simulations [*Daughton*, 2003] have a coherent structure of ion scale while the waves in the experiments [*Ji et al*., 2004] are strongly nolinear with a much shorter coherence length. Given the frequency of the observed electromagnetic fluctuations (about the lower hybrid frequency), we suggested that the observed electromagnetic wave in the flux rope center is one contribution of the LHDI, i.e. the electromagnetic lower-hybrid-frequency-range waves.

Zhou et al., [2009] also show the electromagnetic LHDW at the center of the current sheet and explore their properties, but neglect the electrostatic lower-hybrid-frequency-range waves surrounding the electromagnetic waves. In this paper, we find that the electrostatic and electromagnetic LHDWs are both located inside a large magnetic flux rope, and that the electromagnetic component was mainly confined to the center of the flux rope while the electrostatic components were observed at the edge of the flux rope. In the other flux ropes embedded in the ion diffusion region, however, only the electrostatic lower hybrid-range waves are always detected. The main difference between the last flux ropes and the others is the spatial scale. Since the electromagnetic waves were detected only near the center of the flux rope, the question of whether they can really occur in a broad current sheet, as predicted in simulations [*Daughton et al.*, 2003], is still open. It appears in this event that the waves are

all limited to the inside of the flux ropes.

The core field of magnetic flux ropes is generally supposed to be created by the ambient guide field in magnetic reconnection. As stated in section 3.1, the guide field in this reconnection event directed to the dawn side ($B_g \sim -4\ nT$). However, the core field of the five magnetic flux ropes did not all point to the dawn side. For example, the core field of the third flux rope pointed duskward. Apparently, it cannot be formed by the compression of the ambient guide field [*Huang et al.*, 2012]. In other words, the core field of the flux ropes does not appear to necessarily originate from the background guide field. Since the third flux rope was observed at $B_x > 0$ while the other four flux ropes were detected at $B_x < 0$, the polarity of the core field is consistent with the Hall magnetic field. It indicates that the core field could be created by the compression of the localized Hall magnetic field, in good agreement with the previous observations [*Teh et al.*, 2014; *Wang et al.*, 2016].

Strong broad band waves of higher frequency up to local electron cyclotron frequency were detected inside magnetic flux ropes tens of years ago [*Kennel et al.*, 1986]. Recently, *Khotyaintsev* et al., [2010] reported another interesting event where a series of electron holes were found at the center of one flux rope. In our reconnection event, even though a series of flux ropes are detected within one reconnection diffusion region, the properties of the density, core field, current density and the waves inside each of the flux ropes are different. It means that the microphysics within magnetic flux rope could be complicated. If all of the flux ropes experience a similar evolution in their lifetime, the different properties indicates that the flux ropes were encountered at a different stage. Alternatively, the various B_x values of the flux ropes indicate that the distances between the spacecraft trajectory and the centers of the flux

ropes, i.e. the various "impact parameter" [*Slavin et al*., 2003], are different. Thus, the different properties of the flux ropes could be due to the different regions relative to the axis of the flux ropes where the spacecraft passed through.

In summary, by analyzing the LHRWs associated with a large flux rope observed in a magnetotail reconnection event, we found the electrostatic LHRWs at the edge of and the electromagnetic LHRWs at the center of the largest flux rope. The observation is consistent with the simulation prediction that the LHDW is confined at the current sheet edge but can penetrate into the current sheet center in the form of the electromagnetic mode. The LHRWs are observed in each flux rope filling in the ion diffusion region.

Acknowledgments

R. Wang appreciates the valuable discussion from F. Guo and X. C. Liu at Los Alamos National Laboratory. All Cluster data are available at Cluster Science Archive (http://www.cosmos.esa.int/web/csa). We thank the FGM, CIS, EFW, PEACE, and RAPID instrument teams. This work is supported by the National Science Foundation of China (NSFC) grants (41474126, 41274144, 41174122, and 41421063) and by the National Basic Research Program of China (2014CB845903 and 2013CBA01503). This work at Austria is supported by the Austrian Science Fund (FWF) I2016-N20.

References

Bale, S. D., F. S. Mozer, and T. Phan (2002), Observation of lower hybrid drift instability in the diffusion region at a reconnecting magnetopause, *Geophys. Res. Lett.*, *29*(24), doi:2180 10.1029/2002gl016113.

Balogh, A., et al. (2001), The Cluster Magnetic Field Investigation: overview of in-flight performance and initial results, *Ann. Geophys. 19*(10-12), 1207-1217.

Borg, A. L., M. Oieroset, T. D. Phan, F. S. Mozer, A. Pedersen, C. Mouikis, J. P. McFadden, C. Twitty, A.

Balogh, and H. Reme (2005), Cluster encounter of a magnetic reconnection diffusion region in the near-Earth magnetotail on September 19, 2003, *Geophys. Res. Lett.*, *32*(19), doi: L19105 10.1029/2005gl023794.

Carter, T. A., H. Ji, F. Trintchouk, M. Yamada, and R. M. Kulsrud (2002), Measurement of lower-hybrid drift turbulence in a reconnecting current sheet, *Phys. Rev. Lett.*, *88*(1), doi: 015001 10.1103/PhysRevLett.88.015001.

Cornilleau-Wehrlin, N., et al. (2003), First results obtained by the Cluster STAFF experiment, *Ann. Geophys.*, *21*(2), 437-456.

Daughton, W. (2003), Electromagnetic properties of the lower-hybrid drift instability in a thin current sheet, *Phys. Plasmas*, *10*(8), 3103-3119, doi:10.1063/1.1594724.

Daughton, W., G. Lapenta, and P. Ricci (2004), Nonlinear evolution of the lower-hybrid drift instability in a current sheet, *Phys. Rev. Lett.*, *93*(10), doi:105004 10.1103/PhysRevLett.93.105004.

Daughton, W., V. Roytershteyn, H. Karimabadi, L. Yin, B. J. Albright, B. Bergen, and K. J. Bowers (2011), Role of electron physics in the development of turbulent magnetic reconnection in collisionless plasmas, *Nat. Phys.*, *7*(7), 539-542, doi:10.1038/Nphys1965.

Davidson, R. C., and N. T. Gladd (1975), Anomalous Transport Properties Associated with Lower-Hybrid-Drift Instability, *Phys. Fluids*, *18*(10), 1327-1335, doi: 10.1063/1.861021.

Davidson, R. C., N. T. Gladd, C. S. Wu, and J. D. Huba (1977), Effects of Finite Plasma Beta on Lower-Hybrid-Drift Instability, *Phys. Fluids*, *20*(2), 301-310, doi: 10.1063/1.861867.

Dorfman S., H. Ji, M. Yamada, J. Yoo, E. Lawrence, C. Myers, and T. D. Tharp (2012), Three-dimensional, impulsive magnetic reconnection in a laboratory plasma, *Geophys. Res. Lett.*, 40, 233–238, doi:10.1029/2012GL054574.

Dunlop, M. W., A. Balogh, K. H. Glassmeier, and P. Robert (2002), Four-point Cluster application of magnetic field analysis tools: The Curlometer, *J. Geophys. Res.*, *107*(A11), doi: 1384 10.1029/2001ja005088.

Escoubet, C. P., M. Fehringer, and M. Goldstein (2001), The Cluster mission - Introduction, *Ann. Geophys.*, *19*(10-12), 1197-1200.

Fujimoto, K. (2009), Fast magnetic reconnection in a kinked current sheet, *Phys. Plasmas*, *16*(4), doi: 04210310.1063/1.3106685.

Fujimoto, M., I. Shinohara, and H. Kojima (2011), Reconnection and Waves: A Review with a Perspective, *Space Sci. Rev.*, *160*(1-4), 123-143, doi:10.1007/s11214-011-9807-7.

Guo, F., Q. M. Lu, J. Guo, and S. Wang (2008), Nonlinear evolution of lower-hybrid drift instability in Harris current sheet, *Chinese Phys. Lett.*, *25*(7), 2725-2728.

Gustafsson, G., et al. (2001), First results of electric field and density observations by Cluster EFW based on initial months of operation, *Ann. Geophys.*, *19*(10-12), 1219-1240.

Horiuchi, R., and T. Sato (1999), Three-dimensional particle simulation of plasma instabilities and collisionless reconnection in a current sheet, *Phys. Plasmas*, *6*(12), 4565-4574, doi: 10.1063/1.873744.

Huang, S. Y., et al. (2012), Electron acceleration in the reconnection diffusion region: Cluster observations, *Geophys. Res. Lett.*, *39*, doi: L11103 10.1029/2012gl051946.

Huba, J. D., J. F. Drake, and N. T. Gladd (1980), Lower-Hybrid-Drift Instability in Field Reversed Plasmas, *Phys. Fluids*, *23*(3), 552-561, doi:10.1063/1.863003.

Ji, H. T., S. Terry, M. Yamada, R. Kulsrud, A. Kuritsyn, and Y. Ren (2004), Electromagnetic fluctuations during fast reconnection in a laboratory plasma, *Phys. Rev. Lett.*, *92*(11), doi:11500110.1103/PhysRevLett.92.115001.

Johnstone, A., C. Alsop, S. Burge, P. J. Carter, A. J. Coates, A. J. Coker, A. N. Fazakerley, M. Grande, R. A.

Gowen, and C. Gurgiolo (1997), PEACE: A PLASMA ELECTRON AND CURRENT EXPERIMENT, *Space Sci. Rev.*, *79*(1-2).

Kennel, C. F., F. V. Coroniti, and F. L. Scarf (1986), Plasma-Waves in Magnetotail Flux Ropes, *J. Geophys. Res.*, *91*(A2), 1424-1438, doi: 10.1029/JA091iA02p01424.

Khotyaintsev, Y. V., A. Vaivads, M. Andre, M. Fujimoto, A. Retino, and C. J. Owen (2010), Observations of Slow Electron Holes at a Magnetic Reconnection Site, *Phys. Rev. Lett.*, *105*(16), doi: 16500210.1103/PhysRevLett.105.165002.

Krall, N. A., and P. C. Liewer (1971), Low-Frequency Instabilities in Magnetic Pulses, *Phys. Rev. A*, *4*(5), 2094, doi: 10.1103/PhysRevA.4.2094.

Lin, Y., X. Y. Wang, S. Lu, J. D. Perez, and Q. Lu (2014), Investigation of storm timemagnetotail and ion injection using three-dimensional global hybrid simulation, *J. Geophys. Res.*, *119*(9), doi:10.1002/2014ja020005.

Norgren, C., A. Vaivads, Y. V. Khotyaintsev, and M. Andre (2012), Lower Hybrid Drift Waves: Space Observations, *Phys. Rev. Lett.*, *109*(5), doi: 05500110.1103/PhysRevLett.109.055001.

Pritchett, P. L., F. S. Mozer, and M. Wilber (2012), Intense perpendicular electric fields associated with three-dimensional magnetic reconnection at the subsolar magnetopause, *J. Geophys. Res.*, *117*, doi:A0621210.1029/2012ja017533.

Roytershteyn, V., W. Daughton, H. Karimabadi, and F. S. Mozer (2012), Influence of the Lower-Hybrid Drift Instability on Magnetic Reconnection in Asymmetric Configurations, *Phys. Rev. Lett.*, *108*(18), doi:18500110.1103/PhysRevLett.108.185001.

Roytershteyn, V., S. Dorfman, W. Daughton, H. Ji, M. Yamada, and H. Karimabadi (2013), Electromagnetic instability of thin reconnection layers: Comparison of three-dimensional simulations with MRX observations, *Phys. Plasmas*, *20*(6), doi:06121210.1063/1.4811371.

Schwartz, S. J. (1998), Schock and discontinuity normals, mach numbers, and related parameters, in Analysis Methods for Multi Spacecraft Data, edited by G. Paschmann and P. W. Daly, p. 256, Eur. Space Agency, Bern Switzerland.

Slavin, J. A., R. P. Lepping, J. Gjerloev, D. H. Fairfield, M. Hesse, C. J. Owen, M. B. Moldwin, T. Nagai, A. Ieda, and T. Mukai, Geotail observations of magnetic flux ropes in the plasma sheet, J. Geophys. Res., 108(A1), 1015, doi:10.1029/2002JA009557, 2003.

Sonnerup, B. U. O., Haaland, S. E., and Paschmann, G. (2008), Discontinuity Orientation, Motion, and Thickness, in: Multi-Spacecraft Analysis Methods Revisited, edited by: Paschmann, G. and Daly, P., p. 1–15, ISSI/ESA, Netherlands.

Tanaka, M., and T. Sato (1981), Simulations on Lower Hybrid Drift Instability and Anomalous Resistivity in the Magnetic Neutral Sheet, *J. Geophys. Res.*, *86*(Na7), 5541-5552, doi:10.1029/JA086iA07p05541.

Teh, W.-L., R. Nakamura, H. Karimabadi, W. Baumjohann, and T. L. Zhang (2014), Correlation of core field polarity of magnetotail flux ropes with the IMF By: Reconnection guide field dependency, *J. Geophys. Res.*, 119, 2933–2944, doi:10.1002/2013JA019454.

Vaivads, A., M. Andre, S. C. Buchert, J. E. Wahlund, A. N. Fazakerley, and N. Cornilleau-Wehrlin (2004), Cluster observations of lower hybrid turbulence within thin layers at the magnetopause, *Geophys. Res. Lett.*, *31*(3), doi:L0380410.1029/2003gl018142.

Wang, R.S., Q. Lu, R. Nakamura, C. Huang, A. du, F. Guo, W. L. Teh, M. Wu, S. Lu, and S. Wang (2016), Coalescence of magnetic flux ropes in the ion diffusion region of magnetic reconnection *Nat. Phys.*, *12*. 263–267.

Wang, R. S., A. M. Du, R. Nakamura, Q. M. Lu, Y. V. Khotyaintsev, M. Volwerk, T. L. Zhang, E. A. Kronberg, P.

W. Daly, and A. N. Fazakerley (2013), Observation of multiple sub-cavities adjacent to single separatrix, *Geophys.Res. Lett.*, *40*(11), 2511-2517, doi:10.1002/grl.50537.

Wang, R. S., Q. M. Lu, X. Li, C. Huang, and S. Wang (2010), Observations of energetic electrons up to 200 keV associated with a secondary island near the center of an ion diffusion region: A Cluster case study, *J. Geophys. Res.*, *115*, doi:A1120110.1029/2010ja015473.

Winske, D. (1981), Current-Driven Microinstabilities in a Neutral Sheet, *Phys. Fluids*, *24*(6), 1069-1076, doi:10.1063/1.863485.

Yamada, M., R. Kulsrud, and H. T. Ji (2010), Magnetic reconnection, *Rev. Mod. Phys.*, *82*(1), 603-664, doi:10.1103/RevModPhys.82.603.

Zhou, M., et al. (2009), Observation of waves near lower hybrid frequency in the reconnection region with thin current sheet, *J. Geophys. Res.*, *114*, doi:A0221610.1029/2008ja013427.

Zhou, M., H. Li, X. Deng, S. Huang, Y. Pang, Z. Yuan, X. Xu, and R. Tang (2014), Characteristic distribution and possible roles of waves around the lower hybrid frequency in the magnetotail reconnection region, *J. Geophys. Res.*, 119, 8228–8242, doi:10.1002/2014JA019978.

Zhou, X. Z., Z. Y. Pu, Q. G. Zong, P. Song, S. Y. Fu, J. Wang, and H. Zhang (2009), On the error estimation of multi-spacecraft timing method, Ann. Geophys., 27, 3949–3955.

Figures and Figure Captions

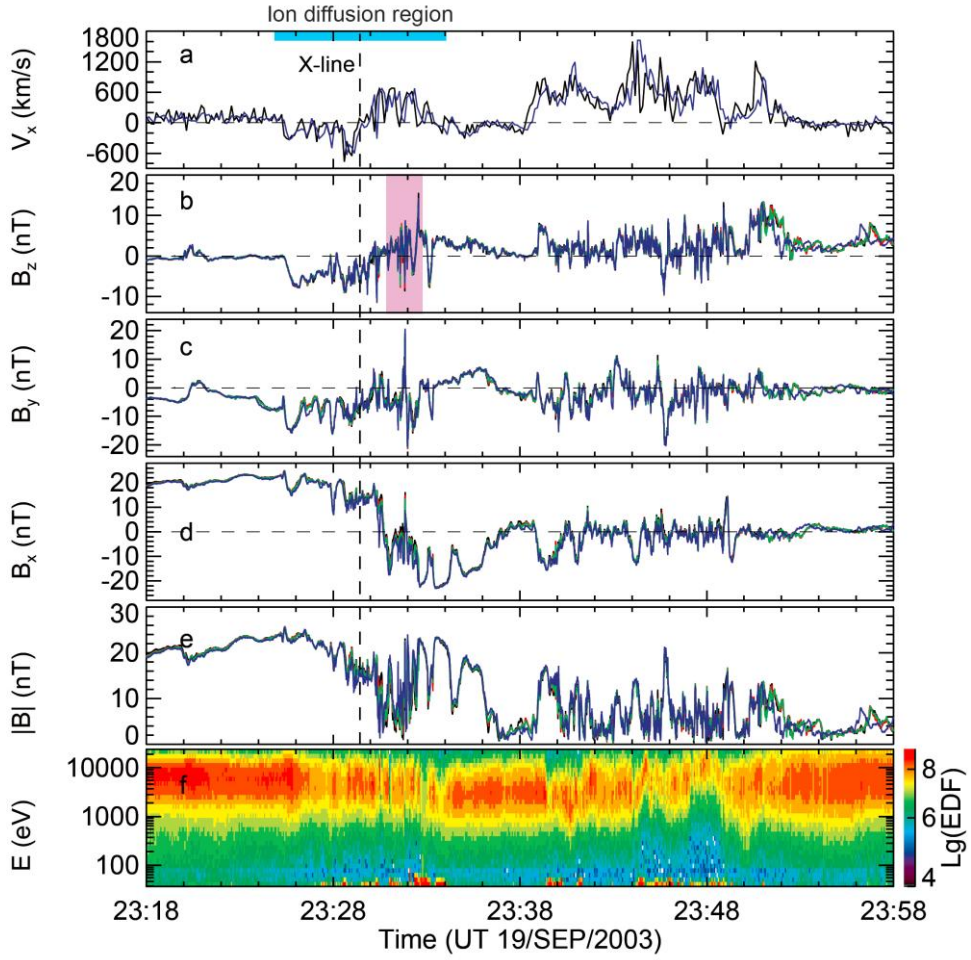

Figure 1. An overview of the reconnection event from the four satellites (C1: black, C2: red, C3: green, C4: blue) of Cluster. (a) ion bulk flows in x direction, (b)-(e) B_z, B_y, B_x and $|\mathrm{B}|$, (f) electron energy spectrum at C4. The horizontal bar at the top corresponds to the interval 23:25-23:34 UT when the ion diffusion region was encountered.

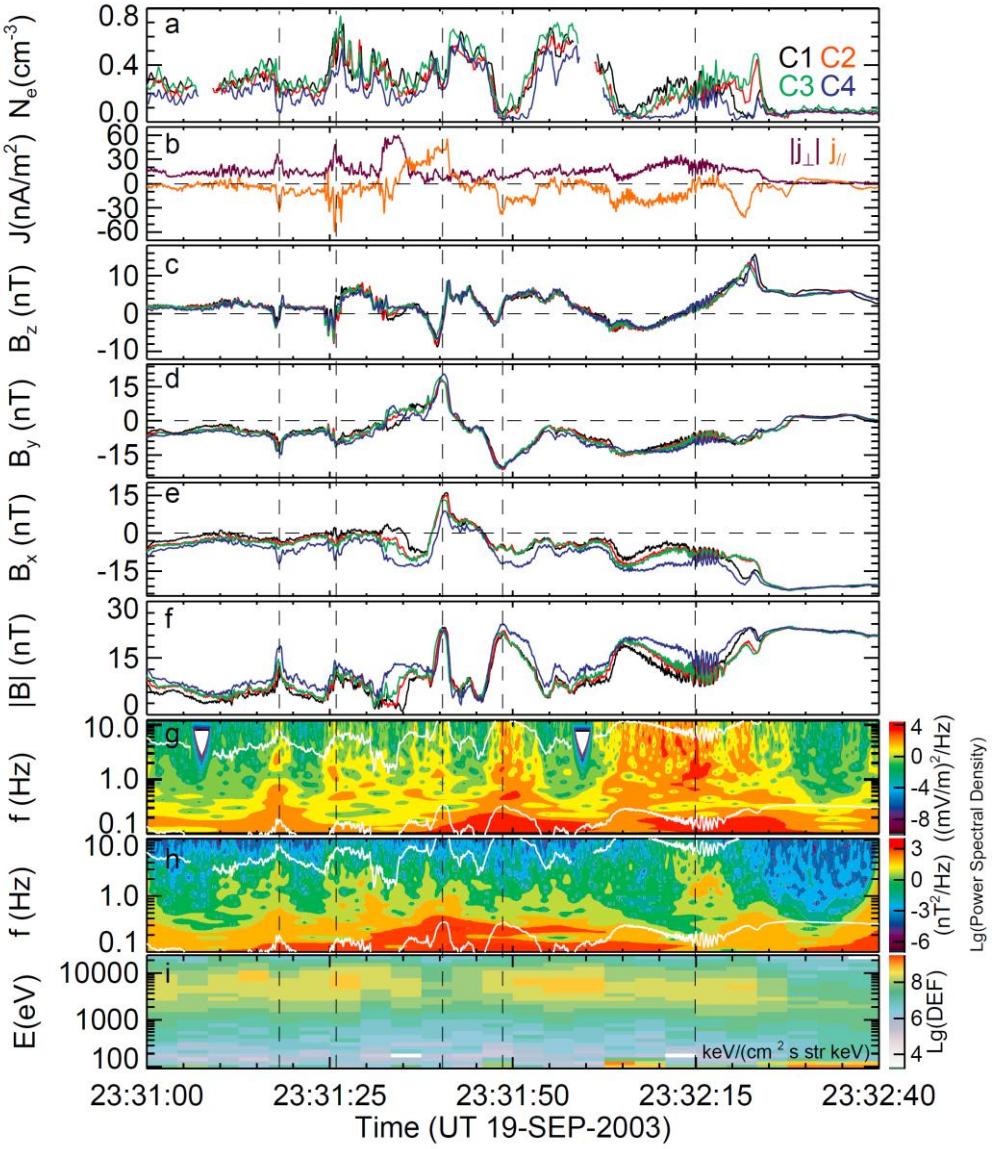

Figure 2.. (a) electron density, (b) absolute values of the current density in the perpendicular direction ($|j_{\perp}|$) and the parallel current density ($j_{//}$), (c)-(f) three components and magnitude of magnetic field, (g)-(h) power spectral density of electric field and magnetic field at C2, (i) electron energy spectrum at C4.

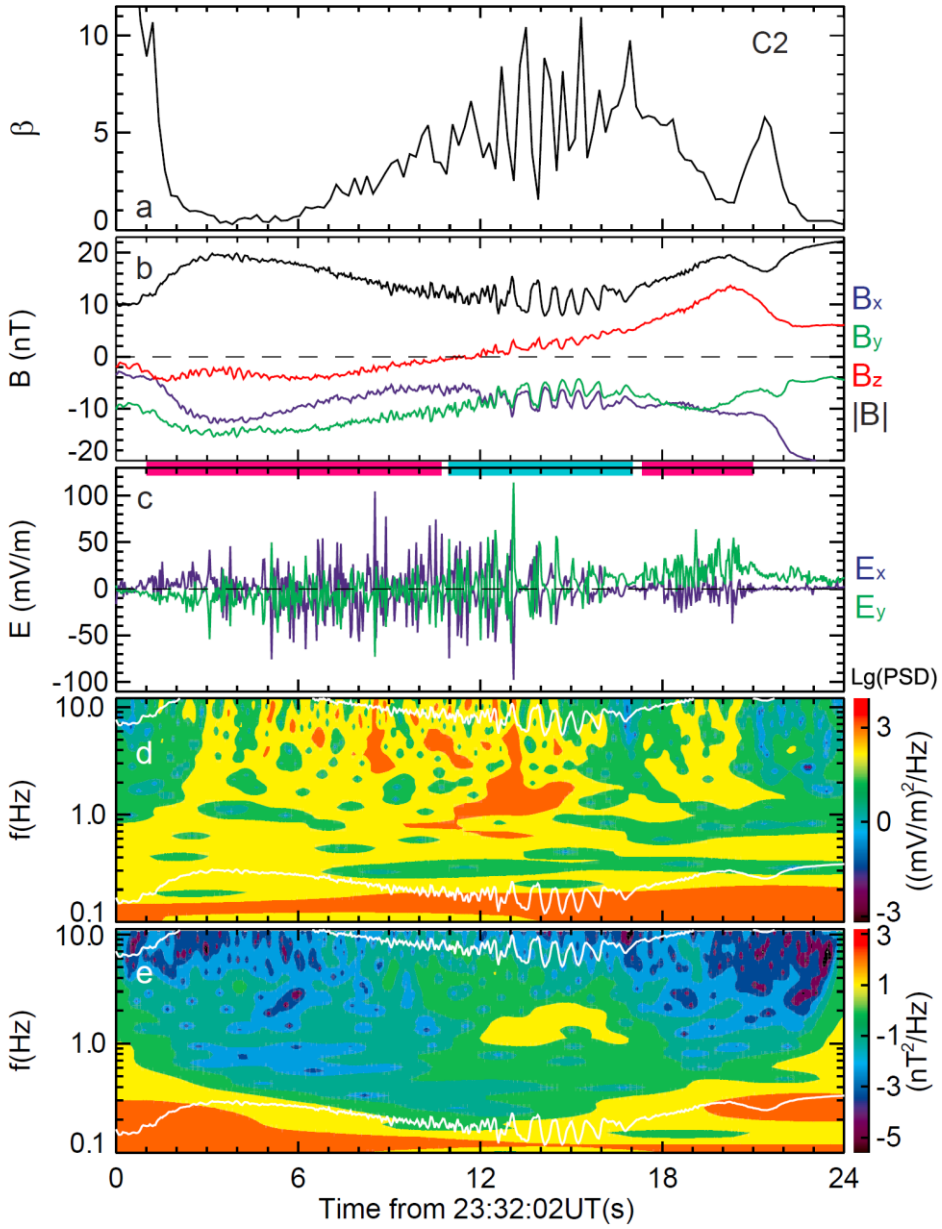

Figure 3. Waves inside the last flux rope at ~23:32:15 UT. (a) plasma beta at C2, the ion temperature at C2 was obtained assuming the ratio between the ion and electron temperature is about 5, (b) B_x: blue, B_y: green, B_z: red, and $|B|$: black, (c) E_x: blue and E_y: green, (d)-(e) power spectral density of magnetic field and electric field.

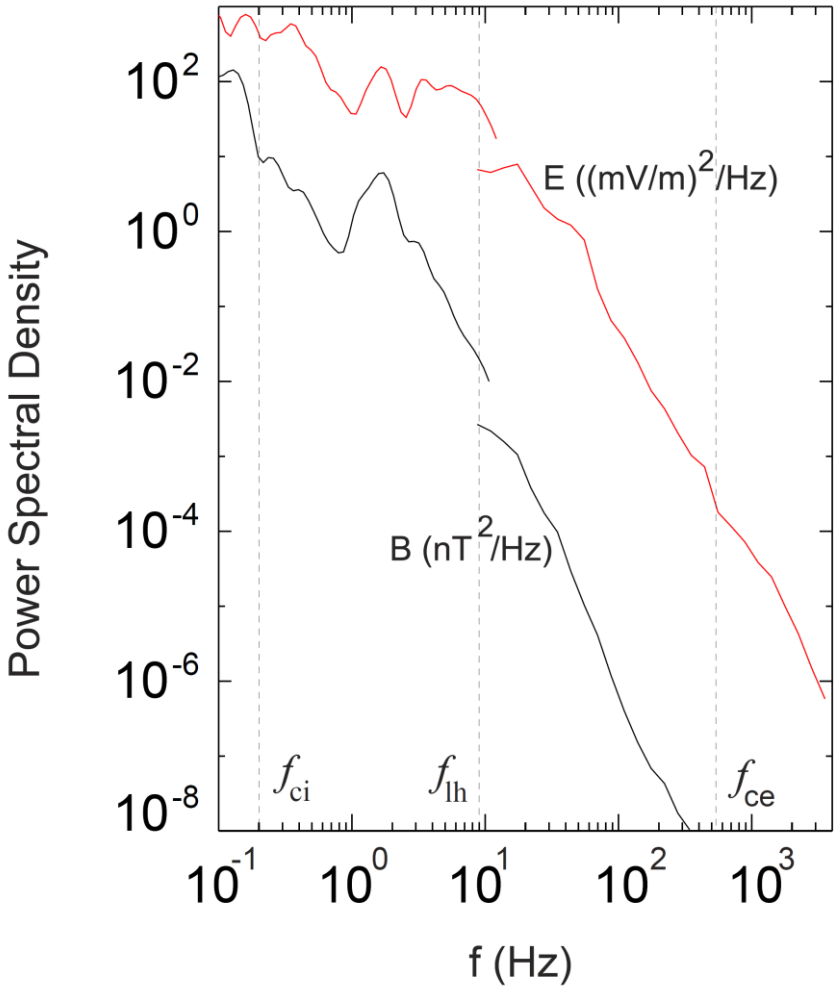

Figure 4. power spectral density of magnetic field (black) and electric field (red)

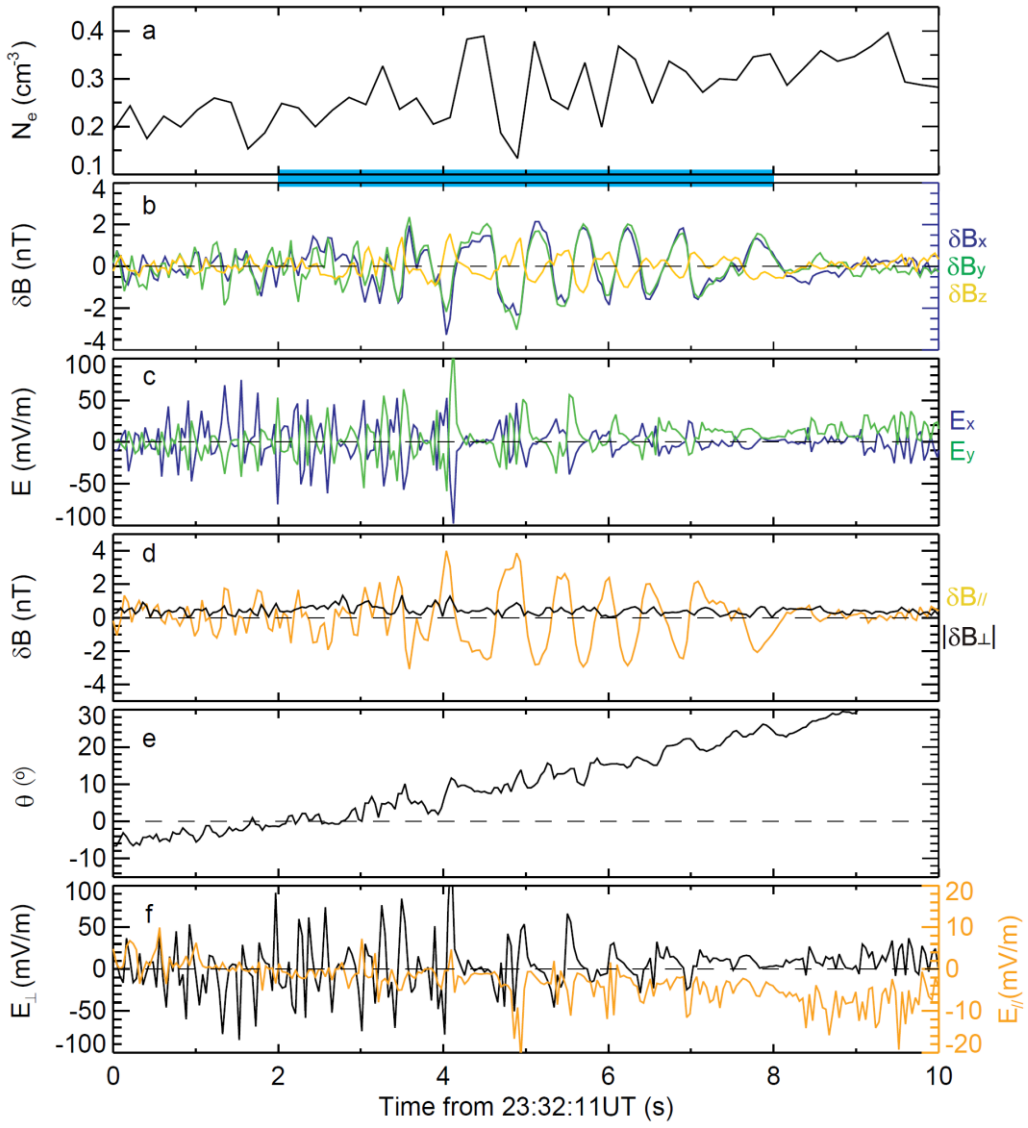

Figure 5. The wave properties at C2. (a) electron density, (b) variation of magnetic field in the three components, (c) electric field in x and y components, (d) variation of magnetic field in parallel and perpendicular directions, (e) the angle between magnetic field and the spacecraft spin plane, (f) the parallel electric field and the perpendicular electric field in y component.

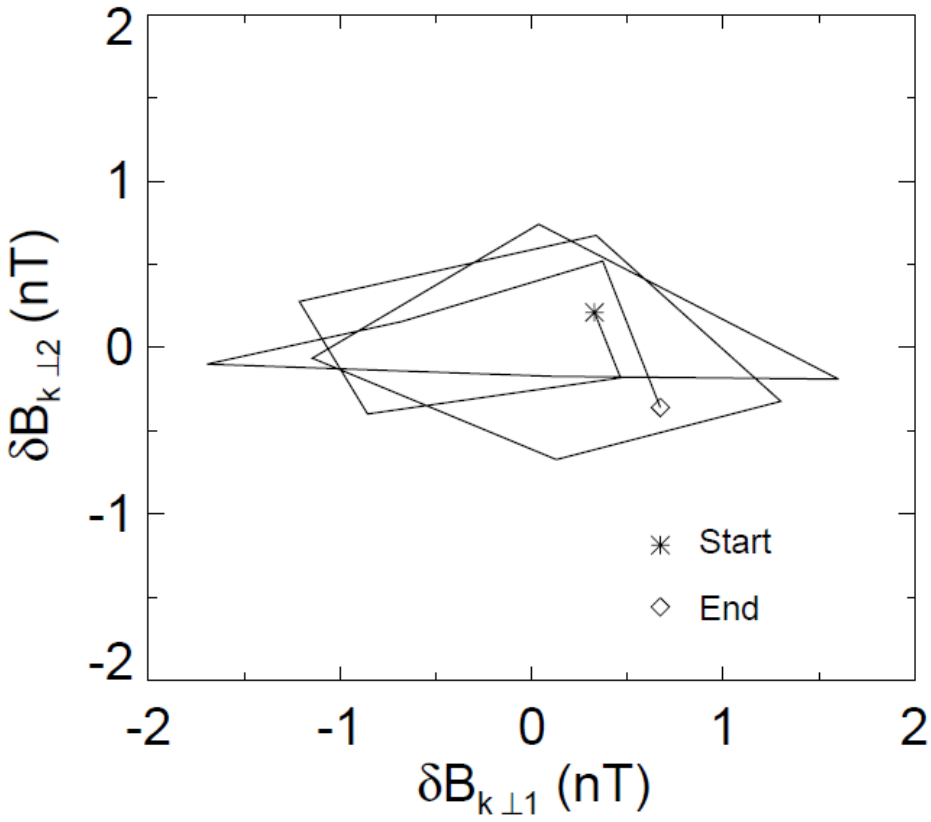

Figure 6. The polarization of the waves, using the magnetic field data in the interval 2332:13.8-2332:14.5 UT.